Soft Matter

Cite this: *Soft Matter*, 2012, **8**, 6582

www.rsc.org/softmatter

PAPER

Assessing structure and dynamics of fibrinogen films on silicon nanofibers: towards hemocompatibility devices

Natalia Hassan,[b] Valeria Verdinelli,[a] Juan M. Ruso[b] and Paula V. Messina*[a]

Received 1st March 2012, Accepted 16th April 2012
DOI: 10.1039/c2sm25489a

An enhanced knowledge of the interaction of proteins with the surfaces of implantable materials, particularly regarding fibrinogen (Fb), is fundamental for understanding cellular events and the overall host response. Thinking of future use of Si-nanofibers as three-dimensional (3D) scaffolds for construction of implantable artificial devices, the correlation among the material surface characteristics and the amount, structure and distribution of adsorbed Fb molecules are analyzed. The Fb adsorption process occurs in a stepwise fashion with an initial rapid adsorption, an intermediate reorganization and finally a second slower adsorption regime over a longer period of time. There is a partial desorption of the protein after the first adsorption process, which demonstrates that this step is reversible until 2×10^4 s. Nevertheless the whole process is irreversible, with a high distortion of the original material morphology. The limiting value for the adsorbed Fb surface concentration is about 270 ± 20 μg dm^{-2}; more than three times the adsorption capacity of non fibrillar, 2D or 3D, scaffolds. The fibrous structure and the similitude in size between the substrate (d = 30–50 nm) and the Fb molecules (47–50 nm) are proposed to be the key to the enhanced adsorption process and the acquired final topography of the material.

1. Introduction

The principle for the design of functional tissue engineering products requires the appropriate scaffolding to mimic the structure and biological functions of the native extracellular matrix (ECM) as much as possible. Hence, scientists have turned to nanotechnology, and specifically to nano-fibers,[1–3] as the solution toward the development of wound repair/care products. The nano-fibrous architecture selectively enhances protein adsorption and also allows more than 1.7 times of osteoblastic cell attachment.[4,5] At present, only a few processing techniques can successfully produce fibers, and the subsequent scaffolds, on the nanoscale.[3] In a previous work,[6] we successfully used a microemulsion system as a nano-reactor for the obtention of Si-nanofibers.

The creation of a proper implantable material requires a fundamental knowledge of the bio-response mechanism from the body and its ultimate effects at the interface of the material surface. Then, to understand the body response to implanted materials, it is insightful to first study the interaction of proteins with solid surfaces. Material–protein association mediates the cell-nanostructured surface communications[7–9] and can result in physiological and pathological changes, including macrophage uptake, blood coagulation, protein aggregation, and complement activation.[10–15]

Here, we evaluated the interaction of previously synthesized Si-nanofibers[6] with the third most abundant protein plasma in blood (fibrinogen, Fb) in order to check the hemocompatibility of the material, looking towards the future use of such nanofibers in three-dimensional scaffolds for the construction of implantable artificial devices. Although in its infancy, the field of silica materials and carbon doped with biological molecules has already exhibited its diversity and potential applications in a selection of modern material science frontiers including biocatalysis, biosensing, drug release, and separation of biological molecules.[16] However, the available studies of the toxicity of silica nano-materials are relatively few, especially compared to the vast number of studies of titanium dioxide or carbon nanotubes. Specifically, the health effects of silica nanoparticles have been evaluated in terms of exposure *via* the respiratory tract, after acute or sub-acute exposure; other exposure routes remain unchecked (*e.g.* blood, skin or gastrointestinal tract).[17] There have been fewer studies related to nano-fibers.

Fibrinogen is one of the most relevant proteins that is adsorbed onto biomaterial surfaces because it takes part in blood coagulation and facilitates adhesion and aggregation of platelets, which are very important properties in the processes of both haemostasis and thrombosis.[18] The adsorption of Fb onto inorganic surfaces has been investigated for many years by a variety of methods. The most common methods are spectroscopic[19–23]

[a]*Department of Chemistry, Universidad Nacional del Sur, INQUISUR-CONICET, (8000) Bahía Blanca, Argentina*
[b]*Soft Matter and Molecular Biophysics Group, Department of Applied Physics, University of Santiago de Compostela, Santiago de Compostela, 15782, Spain. E-mail: pmessina@uns.edu.ar; Fax: +54 291 4595160; Tel: +54 291 4595159*

and microscopic[24–27] techniques that directly provide structural information. Unfortunately, even with the progress of experimental techniques allowing the study of surface phenomena, the adsorption process of this protein is not fully understood. At the same time, most of the adsorption studies done are imprecise; relatively little attention has been placed on the fact that the first layer of biomolecules adsorbed onto the surface undergoes various types of conformational changes and, sometimes, can lead to deviations from the ideal behavior, and thus provide misleading interpretation.[28]

Clearly, such a scenario would require further investigation. So, the aim of this article is the quantitative characterization of the effect that nanoscale surface features of Si-nanofibers (chemistry, morphology, and topography) have on the adsorbed Fb films (amount, structure and distribution). To achieve this goal, a rigorous inspection of adsorption–desorption processes has been performed. Particular attention is paid to the adsorption kinetic process; the parameters that determine the different Fb adsorption dynamic regimes and the effect of different Fb concentrations on pore and intraparticle diffusion rates are evaluated in detail. The study is completed by the inspection of material topography by microscopic methods. The obtained results provide novel information inside the complex Fb adsorption processes, and can address the new challenges evoked by the design of new scaffolds, exhibiting improved biocompatibility and defining the appropriate conditions for the safe use of these materials.

2. Results and discussion

Both in the practical applications and in the theoretical studies of protein adsorption processes, it is important to differentiate between the equilibrium isotherms and the kinetics of the adsorption process.[29]

2.1 Non-equilibrium state system: adsorption kinetics

The rate at which macromolecules adsorb at a sub-saturated interface depends intricately on the interactions between incoming molecules and those previously adsorbed (the structure of the interfacial layer). Therefore, the rate of adsorption can itself be a sensitive probe of the interfacial structure.[30]

2.1.1 Adsorption regimes. Fig. 1 shows the adsorbed density (Γ/μg dm^{-2}) *versus* time evolution, computed from adsorption experiments in which different initial concentrations (C_0/mM) of fibrinogen phosphate buffer solution (PBS) are in contact with the adsorbing surface. The Fb adsorption process is complex, as clearly shown in the adsorption profiles. It appears to occur in a stepwise fashion with an initial rapid adsorption followed by an intermediate reorganization step and finally a second slower adsorption step over a longer period. There is a partial desorption of the protein past the first adsorption process, so the process seems to be quite reversible[31] up to 2×10^4 s. Nevertheless the whole process (9×10^4 s) is irreversible. It can be seen that the diverse protein regimes, in which macromolecules interact differently with the material surface, depend on the initial Fb concentration. For $C_0 = 0.12$ mM, three regimes can be identified: a first adsorption region (0–14 400 s) followed by

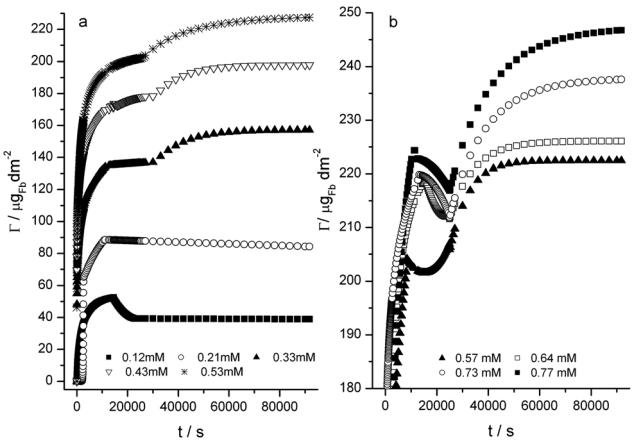

Fig. 1 Profiles of Fb adsorption onto Si-nanofibers at different initial protein solution concentrations, C_0.

desorption until $t = 23\,100$ s, and finally a region where protein surface concentration is constant ($\Gamma = 39.3$ μg dm^{-2}). During the desorption process, about 13.3 μg dm^{-2} of Fb is squeezed from the solid–solution interface. A little increment of the initial protein concentration ($C_0 = 0.21$ mM) causes a great change in the Fb adsorption behavior: two consecutive adsorption steps and a final period where the protein surface concentration is almost constant ($\Gamma \approx 86.4$ μg dm^{-2}) can be identified, while no desorption regimes appeared. For $C_0 = 0.33$ mM, once more three regimes can be observed: (0–12 000 s) protein adsorption until surface saturation ($\Gamma = 134.8$ μg dm^{-2}); (12 000–30 000 s) constant surface concentration; and a final step (30 000–90 000 s) where a new adsorption process takes place until a maximum protein concentration is reached, $\Gamma = 157.5$ μg dm^{-2}. The second layer of protein is presumably adsorbed onto the first layer (not necessarily a compact one) after an induction period where the first protein layer suffers a kind of conformational change, exposing new favorable adsorption sites. For $C_0 = 0.43$ mM and 0.53 mM, two consecutive adsorption processes can be detected. Finally, for $C_0 > 0.53$ mM, protein desorption is again appreciated; the evolution of events can be summarized as follows: a first initial adsorption step (0–8400 s) followed by desorption (8400–24 900 s) to end with a new adsorption process (24 900–90 000 s).

Many kinetics models were developed in order to find intrinsic kinetic adsorption constants. Traditionally, the kinetics of adsorption is described following the expressions originally given by Lagergren,[32] which are special cases for the Langmuir rate equation. The Langmuir equation is based on some quite reasonable assumptions.[33] These are: a uniform surface where the sites of adsorption are energetically equivalent, a single layer of adsorbed material, and a constant temperature. For the system being studied, two of these three conditions are not met. However, some literature findings show some studies of protein adsorption on solid surfaces evaluated by the Langmuir equation.[34] In consideration of the existence of these studies, the Langmuir equation was tested and, as we expected, the theoretical data do not fit the experimental ones. So, we assumed that it is not correct to apply the kinetic equations of Lagergren because they are derived from the Langmuir equation. Nevertheless, we have also tested the Lagergren equations, without satisfactory results. In light of the obtained results, the Fb kinetic

curves on Si-nanofibers were adjusted using Avrami's exponential function:

$$\Gamma(t) = \Gamma_{eq}\left(1 - \exp^{-[k_{av}t]^n}\right) \quad (1)$$

where k_{av} is Avrami's kinetic rate constant and n is the reaction order. This equation allows us to consider in a simple manner many events that are present in the kinetic adsorption of proteins: possible changes in the adsorption rates as a function of the initial supernatant solution concentration and/or the adsorption time, as well as the determination of fractionary kinetic orders.[35,36]

To quantitatively compare the applicability of the applied kinetic model, the normalized standard deviation ($\Delta\Gamma(\%)$) was also calculated.

$$\Delta\Gamma(\%) = 100 \times \sqrt{\frac{\sum\left[\left(\Gamma(t)_{\exp} - \Gamma(t)_{cal}\right)/\Gamma(t)_{\exp}\right]^2}{a-1}} \quad (2)$$

where $\Gamma(t)_{calc}$ is the adsorption capacity calculated values from the Avrami's model and a is the number of experimental points on the kinetic curve.

It was not possible to make a single adjustment of this equation to all experimental data. So, we suspect that more than one adsorption process can exist, which coincides with many reports on the adsorption of proteins.[37] We applied the equation to different sections of the adsorption profiles (every 2500 s) at different initial protein solution concentrations. We found that the same kinetic parameters describe (in the majority of cases) two adsorption steps. The obtained kinetic parameters are summarized in Table 1, $\Delta\Gamma(\%) \approx 0.05$, confirming the applicability of the selected kinetic model. The order (n) and the Avrami kinetic rate constant (k_{av}) are dependent on the initial concentration. This fact agrees with the existence of different processes controlling the adsorption rate. In such cases, in which two adsorption processes are detected, a careful comparison of adsorption kinetic constants shows that the rate of adsorption during the first step greatly exceeds that observed during the second step, while low values of kinetic order are detected. This is evidence of a significant structural rearrangement taking place during the Fb adsorption. The Avrami kinetic models do not provide us with information about the different interaction mechanisms involved during the kinetic regimes.[38] Therefore, we need to resort to more complex models that allow us to understand in much more detail the protein interaction with Si-nanofibers.

We analyze the three regimes of the adsorption process separately by applying different mechanistic models.

2.1.2 Regime I: initial adsorption step. It is generally known that a typical liquid–solid adsorption process involves film diffusion, intraparticle diffusion, and mass action. For physical adsorptions, the mass action is a very rapid process and can be negligible for a kinetic study. Thus, the kinetic process of adsorption is always controlled by liquid film or intraparticle diffusion.[39] Moreover, when a macromolecular solution is placed in contact with an adsorbing substrate under static conditions, the thickness of the boundary layer surrounding the particle should be significant, and the boundary layer resistance or film

Table 1 Kinetic regime parameters[a]

	Regime 1				Regime 2				Regime 3			
C_0/mM	t/s	k_{av}/s^{-1}	n	Γ^1/μg dm^{-2}	t/s	k_{av}/s^{-1}	n	Γ^2/μg dm^{-2}	t/s	k_{av}/s^{-1}	n	Γ^3/μg dm^{-2}
0.12	≤14400	4.45×10^{-4}	0.667	52.6	14400–23100	—	—	39.3	≥23100	—	—	39.3
0.21	≤2800	3.32×10^{-4}	5.864	65.4	2800–10800	2.83×10^{-4}	0.318	88.2	≥10800	—	—	84.2
0.33	≤12000	9.92×10^{-4}	0.359	134.8	12000–30000	—	—	136.9	≥30000	6.00×10^{-5}	1.190	157.5
0.43	≤16200	1.12×10^{-4}	0.198	172.8	16200–30000	2.88×10^{-4}	0.118	178.3	≥30000	6.80×10^{-5}	1.150	197.8
0.53	≤26800	1.19×10^{-3}	0.387	201.3	≥26800	1.17×10^{-4}	0.717	228.4	—	—	—	—
0.57	≤8400	1.17×10^{-3}	0.538	162.0	8400–24900	—	—	160.0	≥24900	8.50×10^{-5}	1.266	176.4
0.64	≤12700	2.50×10^{-5}	0.104	204.1	12700–25200	—	—	198.4	≥25200	1.02×10^{-4}	0.841	222.2
0.73	≤15300	1.02×10^{-3}	0.455	218.8	15300–25200	—	—	212.1	≥25200	1.12×10^{-4}	0.985	226.1
0.77	≤10200	4.40×10^{-4}	0.478	222.7	10200–24900	—	—	217.2	≥24900	1.00×10^{-4}	0.799	246.7
0.82	≤24900	6.5×10^{-3}	0.805	205.4	≥24900	7.50×10^{-5}	1.447	224.2	—	—	—	—

[a] Γ^n (n = 1, 2 and 3) adsorbed density at the end of regime 1, 2 and 3 respectively.

diffusion should be the major driven rate-controlling factor for the initial adsorption.[40]

As we did with the Avrami kinetic adsorption equation, different models were applied to each 2500 s of the adsorption profiles. We have tested several diffusion models such as: the "linear driving force" rate law,[40] which is usually applied to describe mass transfer though a liquid film; the film diffusion mass transfer rate equation presented by Boyd *et al.*;[41] the homogeneous solid diffusion model;[42] the Weber–Morris model;[43] the Dumwald–Wagner model[44] and the double-exponential function model proposed by Wilczak and Keinath.[45] We found that only the Boyd film diffusion and the Weber–Morris intraparticle diffusion models partially adjust to our experimental data with $R^2 = 0.998$.

The film diffusion mass transfer rate equation presented by Boyd *et al.*[41] is:

$$\ln\left(1 - \frac{\Gamma(t)}{\Gamma_{eq}}\right) = -R't, \quad R' \frac{D'_e}{r_0 \Delta r_0 k'} \tag{3}$$

where R' is the liquid film diffusion constant, D'_e is the effective liquid film diffusion coefficient, r_0 is the radius of adsorbent beads, Δr_0 is the thickness of the liquid film and k' is the equilibrium constant of adsorption. A plot of $\ln(1 - \Gamma(t)/\Gamma_{eq})$ *vs.* t should be a straight line with a slope of $-R'$ if the film diffusion is the rate limiting step. Weber and Morris found that in many adsorption processes, solute uptake varies almost proportionally with $t^{1/2}$ rather than with the contact time t.[43]

$$\Gamma(t) = k_{\text{int}} t^{1/2} \tag{4}$$

where k_{int} is the intraparticle diffusion rate. According to eqn (4), a plot of $\Gamma(t)$ *vs.* $t^{1/2}$ should be a straight line with a slope of k_{int} when the intraparticle diffusion is the rate-limiting step.

Fig. 2a and 2b show the film and intraparticle diffusion plots for Fb adsorption onto Si-nanofibers. Both representations give consecutive straight lines with $R^2 \approx 0.998$; film diffusion can be appreciated from 250–2500 s and intraparticle diffusion from 2500 to 10 000 s.

Previously, we said that diffusion models partially adjust to the experimental data because the graphs do not pass through the origin, which means that the intraparticle and/or film diffusion mechanisms are not the only rate controlling steps. Other processes may also occur at the same time, all of which may be operating together. Taking into account the inhomogeneous nature of the protein adsorption process, we consider the possibility of any kind of chemical interaction between adsorbed and pre-adsorbed molecules. So, the reaction models were tested. We previously discarded the pseudo-first-order and pseudo-second-order rate equations proposed by Lagergren.[32] We tested other second order equation models[46] and Elovich's equation,[47] obtaining good results only with the latter. The Elovich equation is satisfied in chemical adsorption processes and is suitable for systems with heterogeneous adsorbing surfaces:

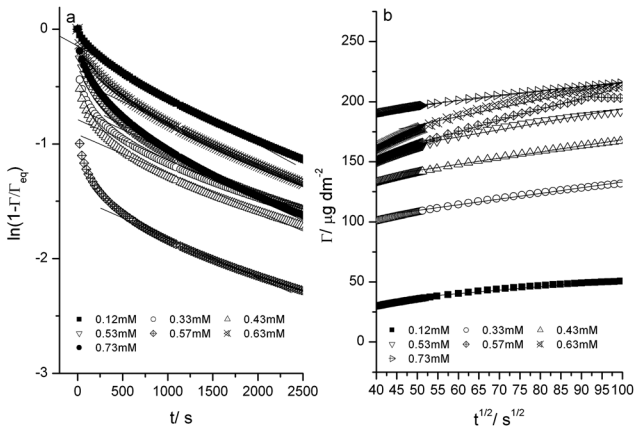

Fig. 2 (**a**) Film and (**b**) intraparticle diffusion plots for Fb adsorption onto Si-nanofibers during the first adsorption step.

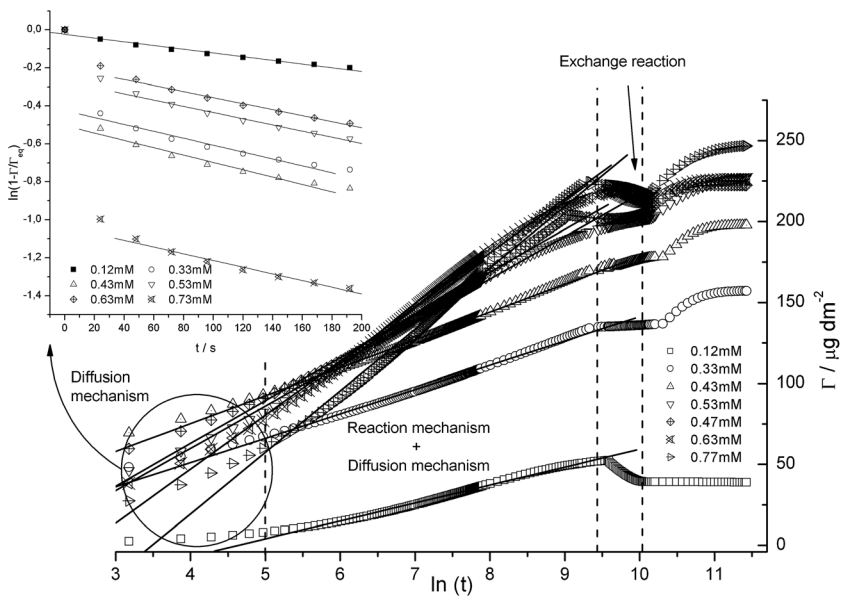

Fig. 3 Fibrinogen adsorption regimes. Inset: representation of film diffusion mass transfer rate equation for the initial 150 s.

$$\frac{d\Gamma(t)}{dt} = ae^{-\alpha\Gamma(t)} \quad (5)$$

where a is the desorption constant and α the initial adsorption rate. With the assumption that $a\alpha\ t \gg 1$[47] and integrating with boundary conditions $\Gamma(t) = 0$ at $t = 0$ and $\Gamma(t) = \Gamma(t)$ at $t = t$, the Elovich rate equation becomes:[46]

$$\Gamma(t) = \alpha\ln(a\alpha) + \alpha\ln(t) \quad (6)$$

Fig. 3 shows the variation of Γ *vs.* $\ln(t)$. It can be seen that such a representation gives a straight line from 150–10 000 s. This is indicative that the Elovich equation is satisfied just with diffusion models. Nevertheless, the reaction model is far away linearly from 0 to 150 s. We again tested the diffusion models in this initial time range and confirmed that film diffusion is applicable, with a straight line that occasionally passes through the origin at low C_0, (inset Fig. 3). As a result, we reason that over the first 150 s, the rate of adsorption is controlled mainly by a film diffusion mechanism. After 150 s of adsorption, reaction mechanisms are also present. The general explanation for this form of kinetic law involves variation of the reaction energetics with the extent of surface coverage. Another plausible explanation could be that active sites are heterogeneous in nature, and therefore exhibit different activation energies. This is in accordance with the existence of a pre-adsorbed layer of protein that exposes new attractive sites for the favorable adsorption of approaching protein molecules. Film diffusion rate control still continues up to 2500s, where intraparticle diffusion control is appreciated (Fig. 2). From 2500s to the end of the first adsorption regime, both the intraparticle diffusion and reaction rate control operate simultaneously (Fig. 3). The obtained parameters of the diffusion methods and Elovich equations are shown in Table 2. From inspection of Table 2 it can be seen that the rate control mechanism is also highly dependent on the initial concentration of the protein solution (C_0). To a deep analysis of such an effect, the variation of diffusion film and intraparticle constants *vs.* C_0 is shown in Fig. 4. The film diffusion constant augments up to a maximum value of 0.45 mM, where a clear increment of intraparticle diffusion appears. At this concentration, an increment of the initial reaction adsorption rate (α) also exists (Table 2), so we conclude that the effect of adsorbed protein layers begins predominantly at 0.45 mM.

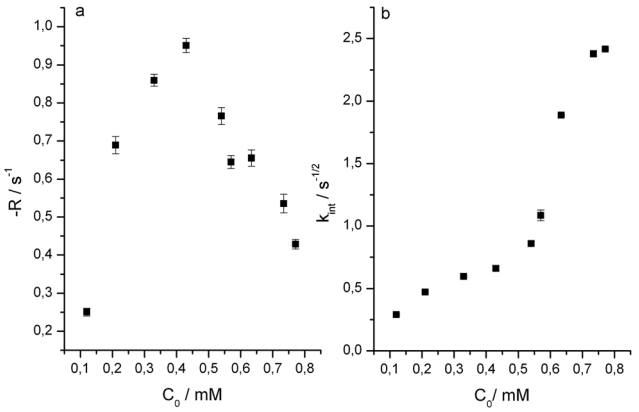

Fig. 4 Dependence of the (**a**) diffusion film coefficient, R, and (**b**) intraparticle constant, k_{int}, on the initial solution protein concentration, C_0.

2.1.3 Regime II: interfacial reorganization. After the first rapid adsorption step (0–10 500s), there is a period of interfacial reorganization which depends on the initial Fb concentration in the bulk solution, as was previously mentioned. In some specific conditions ($C_0 = 0.12$; 0.57; 0.63; 0.73 and 0.77 mM), proteins are squeezed from the interface. Exchange processes of both biopolymers and synthetic polymers adsorbed on surfaces with macromolecules from solution have long been demonstrated;[48] this phenomenon is called an exchange reaction. On the basis of Pefferkorn *et al.*'s[49] experiments, it has been proposed that the exchange reaction rate is related to a rate-limiting step due to the diffusion of macromolecules from bulk through a repulsive barrier formed by a pre-adsorbed species. So, this process could be modeled by a kinetic law depending on both the adsorbed and the bulk molecules.

$$\frac{d[\Gamma^*(t) - \Gamma^*(\infty)]}{dt} = -k_d(C_0)[\Gamma^*(t) - \Gamma^*(\infty)]^{\beta} \quad (7)$$

where $\Gamma^*(t)$ and $\Gamma^*(\infty)$ represent the amount of labeled Fb molecules remaining at the sorbent surface at times t and ∞, respectively, and k_d is the rate constant for desorption. This constant is a function of the concentration of Fb molecules in the solution that is placed in contact with the surface (C_0). The determination of the parameter β and the dependence of k_d on C_0 should furnish useful information about the rate limiting step of the Fb release process.

Table 2 The parameter characterizing regime I, initial adsorption step

	Diffusion models							Reaction models		
	Film diffusion			Intraparticle diffusion				Elovich equation		
C_0/mM	Γ_{eq}/μg dm^{-2}	$-R$/s^{-1}	$-I$	R^2	k_{int}/s$^{-1/2}$	I	R^2	α/μg dm^{-2}	a/dm^2 μg^{-1}	R^2
0.12	52.6 ± 1.4	0.25 ± 0.01	(3.34 ± 0.04)×10^{-4}	0.9888	0.201 ± 0.004	23.0 ± 0.8	0.9855	11.06 ± 0.09	(8.77 ± 0.04)×10^{-4}	0.9950
0.21	88.4 ± 2.2	0.69 ± 0.02	(2.19 ± 0.04) × 10^{-4}	0.9976	0.472 ± 0.005	39.9 ± 0.4	0.9980	17.47 ± 0.28	(7.90 ± 0.06) × 10^{-4}	0.9966
0.33	135.8 ± 3.1	0.86 ± 0.01	(2.65 ± 0.05) × 10^{-4}	0.9757	0.598 ± 0.009	76.9 ± 0.4	0.9895	15.03 ± 0.11	(3.60 ± 0.05) × 10^{-2}	0.9960
0.43	171.9 ± 4.1	0.95 ± 0.02	(2.78 ± 0.08) × 10^{-4}	0.9555	0.607 ± 0.007	109.4 ± 0.4	0.9935	17.21 ± 0.10	(8.40 ± 0.04) × 10^{-2}	0.9970
0.53	204.0 ± 2.3	0.76 ± 0.02	(2.74 ± 0.09) × 10^{-4}	0.9364	0.859 ± 0.018	117.2 ± 0.9	0.9858	26.16 ± 0.16	(6.90 ± 0.04) × 10^{-3}	0.9970
0.57	203.4 ± 9.2	0.64 ± 0.02	(4.14 ± 0.10) × 10^{-4}	0.9698	1.085 ± 0.013	108.3 ± 0.7	0.9949	26.43 ± 0.25	(7.50 ± 0.06) × 10^{-3}	0.9940
0.63	220.4 ± 8.4	0.65 ± 0.02	(3.46 ± 0.09) × 10^{-4}	0.9600	2.642 ± 0.043	56.5 ± 1.4	0.9899	33.39 ± 0.23	(2.50 ± 0.03) × 10^{-3}	0.9970
0.73	218.5 ± 7.5	1.46 ± 0.02	(3.01 ± 0.11) × 10^{-4}	0.9261	2.434 ± 0.005	53.5 ± 0.3	0.9895	33.26 ± 0.04	(4.85 ± 0.14) × 10^{-1}	0.9990
0.77	224.2 ± 9.2	0.43 ± 0.01	(3.49 ± 0.06) × 10^{-4}	0.9840	2.389 ± 0.022	48.6.0 ± 0.9	0.9960	37.97 ± 0.43	(8.06 ± 0.05) × 10^{-4}	0.9910

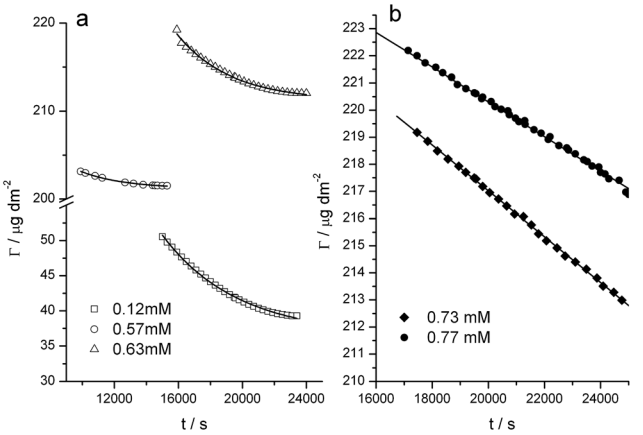

Fig. 5 Fb desorption from Si-nanofibers during the reorganization step. Solid lines are calculated with the (**a**) first and (**b**) zero order kinetic equations.

If we assume that the exchange reaction is a first order kinetic process ($\beta = 1$), as was proposed by Pefferkorn *et al.*,[49] and with the boundary conditions $\Gamma^*(t) = \Gamma^*(0)$ at $t = 0$ and $\Gamma^*(t) = \Gamma^*(t)$ at $t = t$, eqn (7) becomes:

$$\Gamma^*(t) = [\Gamma^*(0) - \Gamma^*(\infty)]e^{-k_1 t} + \Gamma^*(\infty) \quad (8)$$

if $\beta = 2$

$$\frac{1}{\Gamma^*(t) - \Gamma^*(\infty)} = k_d^2 t + \frac{1}{\Gamma^*(0) - \Gamma^*(\infty)} \quad (9)$$

From eqn (8), $\Delta\Gamma^*(t) = \Gamma^*(0) - \Gamma^*(t)$, the amount that has left the surface at time t can be expressed by

$$\Delta\Gamma^*(t) = [\Gamma^*(0) - \Gamma^*(\infty)](1 - e^{-k_1 t}) \quad (10)$$

For the initial protein solution concentrations $C_0 = 0.12$; 0.57 and 0.63 mM, the desorption step was described well by eqn (8) (Fig. 5a), implying a first order kinetic rate control as proposed by Pefferkorn *et al.*[49] The validity of eqn (9) was also tested by plotting the left-hand side of eqn (9) *versus* time. The obtained curve (not shown) was far from the expected linear dependence. Upon increasing C_0 (0.73 and 0.77 mM), the process behaves in a non-exponential way and the characteristic time scale of the exchange process follows a power law independent of the pre-adsorbed molecules (Fig. 5b).

$$\frac{d[\Gamma^*(t) - \Gamma^*(\infty)]}{dt} = -k_d(C_0) \quad (11)$$

Integration of eqn (11) with the same boundary conditions applied to eqn (7) gives:

$$\Gamma^*(t) = -k_d^0 t + \Delta\Gamma^*_\infty + \Gamma^*(\infty), \quad (12)$$

The desorption constants (k_d^1; k_d^0), $\Gamma^*(\infty)$ and $\Delta\Gamma^*_\infty = \Gamma^*(0) - \Gamma^*(\infty)$, are summarized in Table 3. Desorption is significantly increased at high C_0 (high k_d and lower $\Delta\Gamma^*_\infty$ values).

Upon reorganization, hydrophobic surface interactions from the outer layer and possibly from the inner core of the protein may occur. The protein will be distorted as the structure deforms to maximize any such interactions and expose new favorable adsorption sites for the new macromolecules that approach the surface. This is the threshold of the third and final step.

2.1.4 Regime III: final adsorption step. This step is clearly different from the first adsorption (regime I) because of the presence of pre-adsorbed species which are rearranged or removed from the surface. Once the solid–solution interface has been filled to an amount of proteins, where the adsorption step is the limiting rate, the rate of adsorption may be described as proposed by Van Tassel and co-workers:[30]

$$\left(\frac{d\Gamma}{dt}\right)^{((n+1)a)} = k'_a c_b \left[A_0^{(n+1)} + A_1^{(n+1)}\left(\Gamma - \Gamma^{(nd)}\right)\right] - \overline{k}_d\left(\Gamma - \Gamma^{(nd)}\right) \quad (13)$$

where k'_a is the adsorption rate constant, c_b is the concentration of adsorbed molecules from solution, and k_d is the desorption rate constant. The appropriate expansion variable for the $(n + 1)$ th adsorption step is $\Gamma - \Gamma^{(nd)}$, where $\Gamma^{(nd)}$ is the adsorbed density following the nth desorption step and $A_i^{(n)}$ are ith order coefficients.

To characterize this adsorption process, we computed the apparent adsorption rate constants (k'_a) and other parameters from eqn (13). Such parameters are a property of the adsorbate–adsorbent system, and are generally expected to depend on solvent composition (including pH and ionic strength), temperature and pressure. Their values are easily determined from the linear region of the adsorbed density time derivative ($d\Gamma/dt$) *vs.* Γ representation, Fig. 6. The fitted Avrami curves were used to represent the obtained data in the form of ($d\Gamma/dt$) *versus* either time or the adsorbed density. In particular, this latter representation facilitates development of, and comparison to, clear delineation of transport- and reaction-limited regimes.[30] No appreciable differences can be seen for the computed kinetic parameters summarized in Table 4, indicating the independence of second adsorption step behavior with C_0.

Table 3 The parameter characterizing regime II, reorganization step

C_0/mM	k_d^1/s^{-1}	k_d^0/μg dm^2 s^{-1}	$\Gamma^*(\infty)$/μg dm^{-2}	$\Delta\Gamma^*_\infty$ /μg dm^{-2}	R^2
0.12	$(2.00 \pm 0.12) \times 10^{-4}$		36.13 ± 0.84	146.21 ± 1.23	0.9987
0.57	$(2.30 \pm 0.34) \times 10^{-4}$		159.11 ± 4.14	100.21 ± 0.93	0.9998
0.63	$(1.87 \pm 0.23) \times 10^{-4}$		209.33 ± 3.04	88.32 ± 3.23	0.9999
0.73		$(8.45 \pm 0.71) \times 10^{-4}$	201.23 ± 2.05	32.76 ± 2.11	0.9940
0.77		$(6.06 \pm 0.84) \times 10^{-4}$	200.34 ± 2.03	31.99 ± 1.14	0.9920

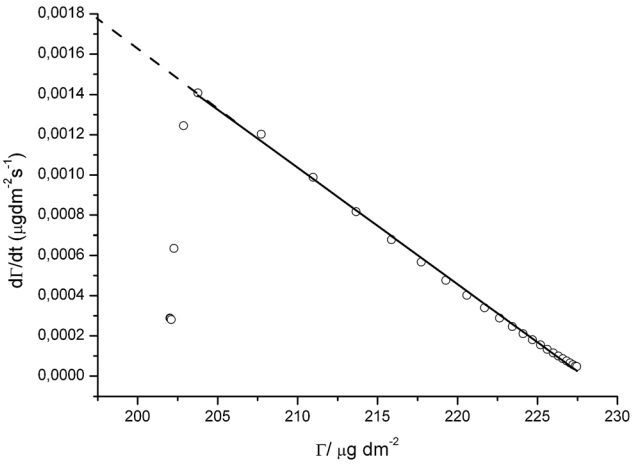

Fig. 6 Illustrative data ($C_0 = 0.77$ mM) of the adsorption rate, $d\Gamma/dt$, *versus* adsorbed density, Γ, during the final adsorption step. The dashed line is a best fit to points in the linear surface-limited regime and used to obtain the parameters summarized in Table 4 using eqn (14), as described in the text.

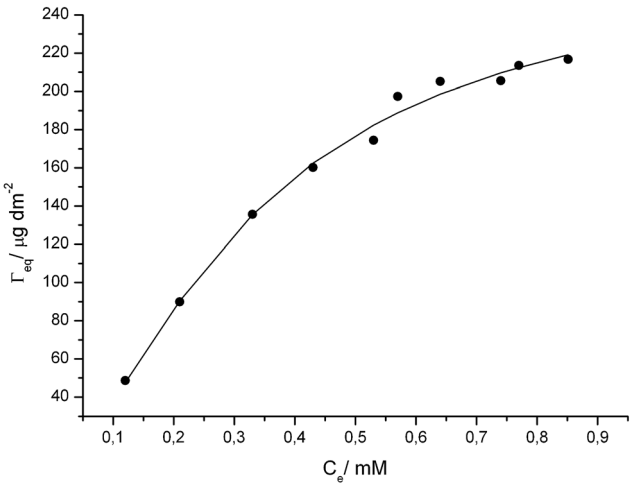

Fig. 7 Black circles: equilibrium adsorption capacity and concentration data. Black line: Sips isotherm adjustments.

2.2 Equilibrium state system: adsorption isotherms

Equilibrium data (at the end of the adsorption process, where no changes in adsorbed protein concentration were detected) were fitted to the Langmuir and Freundlich equations[33,36] with unsatisfactory results. The reason may be found in the heterogeneous nature of this macromolecule adsorption. This surface heterogeneity of the adsorbed protein molecule may arise due either to the energetic heterogeneity of the surface sites, to the heterogeneity of the molecule in the solution, or to a combination of the above reasons.

Rudzinski *et al.*[50] proposed that protein adsorption at equilibrium can be analysed by the Stieltjes transform,[51] based on Sips models, eqn (14).

$$\Gamma_{eq} = \frac{b_s \Gamma_s C_e^{1/n}}{1 + b_s C_e^{1/n}} \quad (14)$$

where Γ_{eq}, C_e, Γ_s, b_s and $1/n$ are the equilibrium adsorption capacity, equilibrium solution concentration, Sips maximum adsorption capacity, equilibrium constant (related to adsorption capacity) and the surface heterogeneity, respectively. The obtained isotherm is shown in Fig. 7. A good agreement ($R^2 \approx 0.998$) is achieved between the theoretical and experimental data. The limiting value for the surface concentration of adsorbed Fb on the Si-nanofibers at the investigated concentrations is about (270 ± 20) μg dm^{-2}, which is highly superior to the data found for the adsorption of such proteins on non-fibrillar, 2D or 3D, substrates (76 μg dm^{-2} on Au; 39 μg dm^{-2} on Si_3N_4; 40–45 μg dm^{-2} on SiO_2 substrates;[28] 60 μg dm^{-2} on hexadecyltrichlorosilane;[52] 80 μg dm^{-2} on nanostructured titania[53]). Estimations of the surface concentration of the fibrinogen ad-layer, assuming an ellipsoidal shape of molecules of 45 nm × 6 nm and lateral dimension results in Γ being approximately 22 μg dm^{-2} and exceeding 150 μg dm^{-2} for side-on and end-on orientations, respectively.[28]

The great adsorption of Fb is supposedly related to the fibrous structure, and not to the material chemistry or the surface topography (porosity). While these last two characteristics are very important for an adsorption process, they do not seem to be the predominant effect because the Si-fibrils do not have porosity or high surface area values. In addition, the Fb adsorption onto siliceous materials has been exceedingly studied and it is known that the interface wettability has a critical influence on the process. At pH 7.4 this protein is adsorbed better onto hydrophobic surfaces.[18,54] On the contrary, in our cases, the tested Si-nanofibers possess a high concentration of hydroxyl groups on their surfaces,[6] through which they can bind to solution water molecules, showing a high hydrophilicity.

The studied fibrillar material is 30–50 nm in diameter (Fig. 8a) and more than 20 μm in length. Such dimensions are of the order of the structural ECM fibers (50–500 nm diameter)[3] and also similar to a Fb molecule (47 nm diameter)[18] in size. The

Table 4 The parameter characterizing regime III, final adsorption step

C_0/mM	k'_d/dm s^{-1}	$A_0{}^{n+1}$	$A_1{}^{n+1}$/dm^2 μg^{-1}	Γ^{nd}/μg dm^2	k_d/s^{-1}	R^2
0.33	$(4.00 \pm 0.32) \times 10^{-4}$	-0.009 ± 0.004	$(7.50 \pm 0.12) \times 10^3$	186.18 ± 3.67	120.06 ± 2.31	0.9992
0.43	$(1.00 \pm 0.12) \times 10^{-4}$	0.006 ± 0.001	$(7.80 \pm 0.16) \times 10^3$	197.00 ± 8.34	116.03 ± 1.12	0.9993
0.53	$(9.00 \pm 0.65) \times 10^{-5}$	0.003 ± 0.001	$(7.40 \pm 0.21) \times 10^3$	227.07 ± 6.12	227.07 ± 2.18	0.9983
0.57	$(9.00 \pm 0.72) \times 10^{-4}$	-0.007 ± 0.004	$(7.30 \pm 0.15) \times 10^3$	223.37 ± 1.34	126.31 ± 1.31	0.9390
0.63	$(9.00 \pm 0.23) \times 10^{-4}$	0.003 ± 0.003	$(7.06 \pm 0.18) \times 10^3$	225.55 ± 3.41	131.30 ± 2.01	0.9987
0.73	$(8.00 \pm 0.76) \times 10^{-4}$	-0.006 ± 0.002	$(6.66 \pm 0.21) \times 10^3$	239.46 ± 2.12	140.30 ± 0.90	0.9999
0.77	$(8.00 \pm 0.13) \times 10^{-4}$	0.008 ± 0.003	$(6.67 \pm 0.12) \times 10^3$	244.29 ± 3.91	140.00 ± 0.91	0.9988

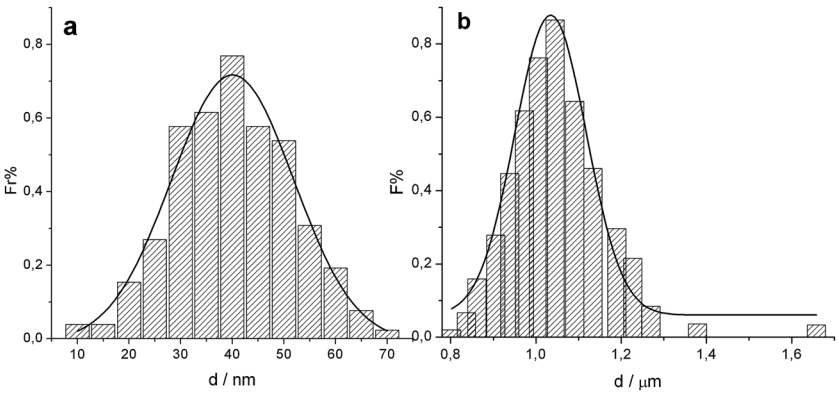

Fig. 8 Size analyses of SEM images for Si-nanofibers (a) before and (b) after equilibrium Fb adsorption.

similitude in size may be the key to the enhancement of the adsorption process. Similar results were obtained by Woo *et al.*;[4] they found that scaffolds with nano-fibrous pore walls adsorbed four times more serum protein than scaffolds with solid pore walls. To evaluate the protein effect on Si-nanofibers, we inspected the material morphology before and after Fb adsorption by scanning electron microscopy.

2.3 Protein adsorption effect on the nanometre-scale material morphology

We analyzed and compared the adsorbent structures after Fb adsorption. It has been noticed that the original SiO_2 fibrillar structure (Fig. 9a) was wrecked. In some cases new fibrillar structures of higher dimensions (d ≈ 1μm, Fig. 8b) are observed (Fig. 9b, 9c and 9d) and in others bicontinuous structures appeared (Fig. 9e and 9f). Manifestly, fibrinogen acts as an agglutinative of the Si-nanofibrils. The interfacial ordering of protein residues seems to be the hallmark of a weak and labile electrostatic attraction between the substrate and the adsorbed macromolecule. Fb is net negatively charged at pH 7.4 (isoelectric point, IP = 5.5[55]), with the highest density of negatively charged residues on the E and D-domains; the αC-domains which are rich in Arg and Lys residues are positively charged.[56] Additionally, the hydropathic index for Fb indicates that the E and D-domains are substantially more hydrophobic than the αC-domains.[56] During adsorption, the αC-domains that tend to be non-covalently tethered to the E-domains[57] disconnect on the way to interact with the hydrophilic and negatively charged Si-nanofibers (see Scheme 1). Literature information indicates that fibrinogen adsorption on 2D solid surfaces occurs basically in two different orientations: "side-on" (laying on the surface) and "end-on" (standing on the surface).[58,59] In both cases, the availability of αC-domains for interaction with the neighboring adsorbed Fb molecules promotes lateral associations and the formation of an extensive network assembly between Si-nanofibers, similar to those that exist during the conversion of fibrinogen into polymeric fibrin.[57] The stochastic adsorption of the protein molecule leads to the formation of two different structures, as can be seen in Fig. 9. The adsorption through a side-end molecular orientation (Scheme 1, A) favors both lateral and equilateral interactions, generating large fibers and bicontinuous structures respectively, while the side-on adsorption (Scheme 1, B) promotes only equilateral interaction and therefore bicontinous structures.

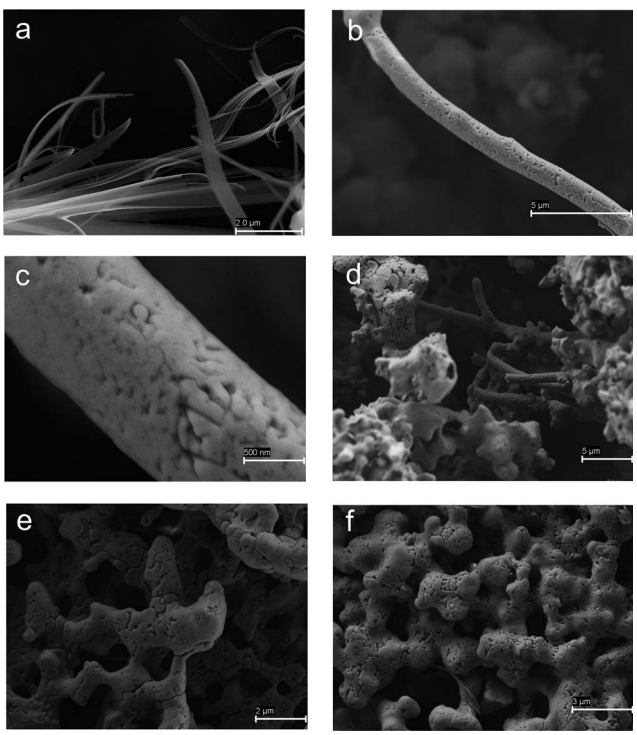

Fig. 9 SEM microphotographs of (a) Si-nanofibers before Fb adsorption; (b, c, d) fibre structure and (e, f) bicontinuous materials obtained after equilibrium Fb adsorption.

3. Experimental

3.1 Material and methods

Sodium bis(2-ethylhexyl) sulfosuccinate (Aerosol OT, 99% Sigma), cyclohexane (Merck, δ = 0.776 g cm^{-3}) and tetraethyl orthosilicate (TEOS, Aldrich 98%) were used without further purification. The Si-nanofibers were synthesized by a microemulsion templated route, following a previously described procedure.[6] For microemulsion preparation, only triply-distilled water was used.

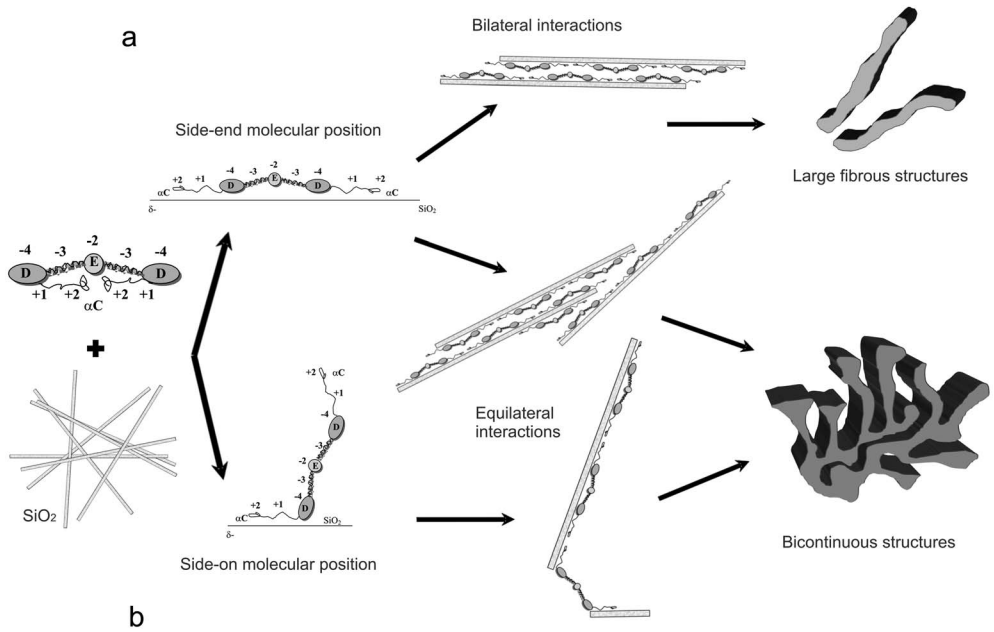

Scheme 1 Schematic representation of Fb–material interaction.

Fibrinogen fraction I, type IV from bovine plasma (F8630) was obtained from Sigma (CAS Number: 9001-32-5). The proper amount of Fb was dissolved in phosphate buffered saline (PBS, Na_2HPO_4/NaH_2PO_4) to approach physiological conditions, pH = 7.4 for 60 min. Phosphate was preferred to tris(hydroxymethyl)aminomethane buffer because the co-adsorption of the small organic molecule and its interference with the experiments had been confirmed. The Fb solution (1 mM) was prepared, stored at −20 °C and diluted as required. Before the beginning of an experiment, Fb solutions were stored at room temperature for a maximum of 1 h.

3.2 Adsorption experiments

The adsorption experiments (in darkness to avoid photodegradation) were carried out *in situ* in an UV-vis-NIR scanning spectrophotometer (Varian Cary 100 Bio) provided with a temperature controller (UV09005M013), using a 1 cm path length rectangular quartz cell. For this, 20 mg of adsorbent was in contact with 3 mL of Fb buffer solutions of different concentrations at 37 °C. The supernatant concentration before and after adsorption was analyzed at λ = 280 nm following the emission of the tryptophan (Trp) group. A scan over a narrow range of wavelengths yielded a measurement every *ca.* 0.4 min, with a precision of 0.02 nm. A mass balance was applied to calculate the protein adsorbed onto Si-nanofibers. The adsorbed density, Γ (μg dm^{-2}) was calculated using the equation:

$$\Gamma = \frac{(C_0 - C)V}{m} S \qquad (15)$$

where C_0 is the protein initial concentration, C the residual concentration at time t, V the solution volume, m the adsorbent mass and S the material BET surface area (0.93 g m^{-2}, measured at 77. 6 K with a Micromeritics Model Accelerated Surface Area and Porosimetry System (ASAP) 2020 instrument. Each sample was degassed at 373 K for 720 min at a pressure of 10^{-4} Pa).

The curves were highly reproducible: each experiment was done three times; the standard deviation on Γ was estimated[60] to be 0.01 μg dm^{-2}.

3.3 Scanning electron microscopy

Field emission scanning electron microscopy (FE-SEM) was performed using a FE-SEM ULTRA PLUS. This instrument operates in high vacuum, enabling work to high resolution levels (0.8 nm at 30 kV) and low voltage in samples without staining (0.02V–30kV, continuously adjusted in steps of 10 volts). Magnification range 12–1 000 000×; sizes of openings: 7.5 μm, 10 μm, 20 μm, 30 μm, 60 μm and 120 μm.

4. Conclusions

By exhaustive analysis of the fibrinogen adsorption process under dynamic and static conditions, we can construct a clear picture of how the Si-nanofiber surface features critically influence the amount, structure and distribution of the protein molecules attached to the material surface. As is evident from the inspection of the adsorption profiles, the Fb adsorption process on the Si-nanofibers is complex and occurs in a stepwise fashion, with an initial rapid adsorption controlled exclusively by diffusion mechanisms. The presence of pre-adsorbed proteins at the interface, after the first 150 s of adsorption, involves the variation of the surface energy with the extent of surface coverage and manifestation of the reaction mechanisms. After the initial adsorption step, there is an intermediate reorganization followed by a second slower adsorption regime over a longer time period. The first adsorption and the reorganization steps highly depend on the initial concentration of the Fb solution (C_0), and are reversible processes. The effect of the adsorbed protein layers

begins predominantly at $C_0 = 0.45$ mM where there is a clear increase in the initial reaction adsorption rate. During the reorganization step, protein desorption was appreciated at high and very low C_0. At low solution concentration, desorption follows a first order kinetic mechanism, while at high concentration the process is independent of pre-adsorbed protein molecules.

The whole Fb adsorption process is irreversible, with a high distortion of the original material morphology. The limiting value for the adsorbed Fb surface concentration is about (270 ± 20) μg dm^{-2}. From inspection of the material morphology before and after Fb adsorption by scanning electron microscopy, it was seen that after protein interaction the original fibrous structure was wrecked, giving rise to fibers of higher dimensions or bicontinuous structures. The fibrous structure and the similitude in size between the fibrous substrate (d = 30–50 nm) and the Fb molecules (47–50 nm), is proposed to be the key to the enhanced adsorption process. After adsorption, the αC-domains are presumably available for interaction with the domains of the neighboring adsorbed Fb molecules, thereby promoting lateral and equilateral associations and the formation of an extensive network similar to those that exist in nature between fibrin units.

These studies have the potential to give out the basis for new material designs in which hemocompatibility is the key factor.

Acknowledgements

The authors acknowledge Universidad Nacional del Sur (PGI 24/ZQ07), Concejo Nacional de Investigaciones Científicas y Técnicas de la República Argentina (CONICET, PIP -11220100100072.), Xunta de Galicia (Project No. 10PXIB206258PR), and Education Audiovisual Culture, Executive Agency European Commission (EMUNDUS18) for their financial support. VV has a postdoctoral fellowship of CONICET. PM is an adjunct researcher of CONICET.

References

1 J. A. Hubbel, *Curr. Opin. Biotechnol.*, 2003, **14**, 551.
2 Z. Ma, M. Kotaki, R. Inai and S. Ramakrishna, *Tissue Eng.*, 2005, **11**(1,2), 101.
3 C. P. Barnes, S. A. Sell, E. D. Boland, D. G. Simpson and G. L. Bowlin, *Adv. Drug Delivery Rev.*, 2007, **59**, 1413 and references therein.
4 K. M. Woo, V. C. Chen and P. X. Ma, *Nano-fibers and proteins*, 2003, **67**, 531.
5 R. L. Price, M. C. Waid, K. M. Haberstroh and T. J. Webster, *Biomaterials*, 2003, **24**, 1877.
6 N. Hassan, V. Verdinelli, J. M. Ruso and P. V. Messina, *Langmuir*, 2011, **27**(14), 8905.
7 M. S. Ehrenberg, A. E. Friedman, J. N. Finkelstein and G. Oberdörster, *Biomaterials*, 2009, **30**, 603.
8 A. E. Nel, L. Madler, D. Velegol, T. Xia and E. M. V. Hock, *Nat. Mater.*, 2009, **8**, 543.
9 M. P. Lutolf, P. M. Gilbert and H. M. Blau, *Nature*, 2009, **426**, 433.
10 Z. J. Deng, M. Liang, M. Monteiro, I. Toth and R. F. Minchin, *Nat. Nanotechnol.*, 2011, **6**, 39.
11 M. S. Ehrenberg, A. E. Friedman, J. N. Finkelstein, G. Oberdorster and J. L. Mc Grath, *Biomaterials*, 2009, **30**, 603.
12 H. C. Fischer and W. C. Chan, *Curr. Opin. Biotechnol.*, 2007, **18**, 565.
13 I. Lynch, A. Salvati and K. A. Dawson, *Nat. Nanotechnol.*, 2009, **4**, 546.
14 I. Lynch and K. A. Dawson, *Nano Today*, 2008, **3**, 40.
15 Z. J. Deng, G. Mortimer, T. Schiller, A. Musumeci, D. Martin and R. F. Minchin, *Nanotechnology*, 2009, **20**, 455101.
16 M. Hartmann, *Chem. Mater.*, 2005, **17**, 4577 and references therein.
17 D. Napierska, L. C. J. Thomassen, D. Lison, J. A. Martens and P. H. Hoet, *Particle and fiber toxicology*, 2010, **7**(39), 1 and references therein.
18 S. Tunc, M. F. Maitz, G. Steiner, L. Vázquez, M. T. Pham and R. Salzer, *Colloids Surf., B*, 2005, **42**, 219 and references therein.
19 G. Steiner, S. Tunc, M. Maitz and R. Salzer, *Anal. Chem.*, 2007, **79**, 1311.
20 Z. J. Deng, M. Liang, M. Monteiro, I. Toth and R. Minchin, *Nat. Nanotechnol.*, 2011, **6**, 39.
21 A. Toscano and M. M. Santore, *Langmuir*, 2006, **22**, 2588.
22 A. V. Bychkova, O. N. Sorokina, A. L. Kovarski, A. B. Shapiro, V. B. Leonova and M. A. Rozenfeld, *Biophysics*, 2010, **55**, 544.
23 N. P. Podolnikova, I. S. Yermolenko, A. Fuhrmann, V. K. Lishka, S. Magonov, B. Bowen, J. Enderlein, A. V. Podolnikov, R. Ros and T. P. Ugarova, *Biochemistry*, 2010, **49**, 68.
24 N. Hassan, J. Maldonado-Valderrama, P. A. Gunning, V. J. Morris and J. M. Ruso, *Colloids Surf., B*, 2011, **87**, 489.
25 N. Hassan, J. Maldonado-Valderrama, P. A. Gunning, V. J. Morris and J. M. Ruso, *J. Phys. Chem. B*, 2011, **115**, 6304.
26 L.-C. Xu and C. A. Siedlecki, *Langmuir*, 2009, **25**, 3675.
27 M. Wasilewska and Z. Adamczyk, *Langmuir*, 2011, **27**, 686.
28 B. A. Snopok and E. V. Kostyukevich, *Anal. Biochem.*, 2006, **348**, 222.
29 F. Fang, J. Satulovsky and I. Szleifer, *Biophys. J.*, 2005, **89**, 1516.
30 Y. Tie, C. Calonder and P. R. Van Tassel, *J. Colloid Interface Sci.*, 2003, **268**, 1.
31 P. Schaaf, Ph. Déjardin, A. Johner and A. Schmitt, *Langmuir*, 1992, **8**, 514.
32 Y. S. Ho and G. Mc Kay, *Process Biochem.*, 2003, **38**, 1047.
33 I. Langmuir, *J. Am. Chem. Soc.*, 1916, **38**, 2221.
34 C. M. Alves, R. L. Reis and J. A. Hunt, *J. R. Soc. Interface*, 2010, **7**, 1367 and references therein.
35 A. R. Cestari, E. F. S. Vieira, J. D. S. Matos and D. S. C. dos Anjos, *J. Colloid Interface Sci.*, 2005, **285**, 288.
36 C. E. Zubieta, P. V. Messina, K. Luengo, M. Dennehy, O. Pieroni and P. Schulz, *J. Hazard. Mater.*, 2008, **152**, 765.
37 A. Katiyar, L. Ji, P. Smirniotis and N. Pinto, *Microporous Mesoporous Mater.*, 2005, **80**, 311.
38 A. R. Cestari, E. F. S. Vieira, A. A. Pinto and F. C. da Roda, *J. Colloid Interface Sci.*, 2008, **327**, 267.
39 H. Qiu, L. Lv, B.-C. Pan, Q.-J. Zhang, W.-M. Zhang and Q.-X. Zhang, *J. Zhejiang Univ., Sci., A*, 2009, **10**, 716.
40 J. A. Chin, S. M. Slack in Biomaterials: Protein-Surface Interactions, *The Biomedical Engineering Handbook*, ed. J. D. Bronzino, CRC Press LLC, Boca Raton, Florida 2nd edn, 2000, ch. 111.
41 G. E. Boyd, A. W. Adamson and L. S. Myers, *J. Am. Chem. Soc.*, 1947, **69**, 2836.
42 D. O. Cooney in *Adsorption Design for Wastewater Treatment*, Lewis Publishers, Boca Raton, Florida, 1999.
43 M. Alkan, Ö. Demirbaş and M. Doğan, *Microporous Mesoporous Mater.*, 2007, **101**, 388.
44 H. L. Wang, J. L. Cheng and Z. C. Zhai, *Environmental Chemistry*, 2004, **23**, 188.
45 A. Wilczak and T. M. Keinath, *Water Environ. Res.*, 1993, **65**, 238.
46 Y. S. Ho, *J. Hazard. Mater.*, 2006, **136**(3), 103.
47 S. H. Chien and W. R. Clayton, *Soil Sci. Soc. Am. J.*, 1980, **44**, 265–268.
48 V. Ball, A. Bentaleb, J. Hemmerle, J.-C. Voegel and P. Schaaf, *Langmuir*, 1996, **12**, 1614 and references therein.
49 E. Pefferkorn, A. Carroy and R. Varoqui, *J. Polym. Sci., Polym. Phys. Ed.*, 1985, **23**, 1997.
50 W. Rudzinski, L. Lattar, J. Zajac, E. Wofram and J. Paszli, *J. Colloid Interface Sci.*, 1983, **96**, 630.
51 A. Sadana, *Chem. Rev.*, 1992, **92**, 1799.
52 C. F. Wertz and M. M. Santore, *Langmuir*, 1999, **15**, 8884.
53 P. E. Scopelliti, A. Borgonovo, M. Indrieri, L. Giorgetti, G. Bongiorno, R. Carbone, A. Podestá and P. Milani, *PLoS One*, 2010, **5**(7), e11862(1).
54 P. Roach, D. Farrar and C. C. Perry, *J. Am. Chem. Soc.*, 2006, **128**, 3939.
55 J. Armstrong, H. J. Salacinski, Q. Mu, A. M. Seifalian, L. Pell, N. Freeman, C. M. Holt and J. R. Lu, *J. Phys.: Condens. Matter*, 2004, **16**, S2483.

56 S.-Y. Jung, S.-M. Lim, F. G. AlbertorioKim, M. C. Gurau, R. D. Yang, M. A. Holden and P. S. Cremer, *J. Am. Chem. Soc.*, 2003, **125**, 12782 and references therein.
57 M. W. Mosesson, *J. Thromb. Haemostasis*, 2005, **3**, 1894.
58 Z. Adamczyk, J. Barbasz and M. Cieśla, *Langmuir*, 2011, **27**, 6868.
59 T. Riedel, J. Suttnar, E. Brynda, M. Houska, L. Medved and J. E. Dyr, *Blood*, 2011, **5**, 1700.
60 J. R. Taylor, in *An Introduction to Error Analysis, The study of Uncertainties in Physical Measurements*, University Science Books, Mills Valley, CA, 1982.

Addition and correction

Note from RSC Publishing

This article was originally published with incorrect page numbers. This is the corrected, final version.

The Royal Society of Chemistry apologises for these errors and any consequent inconvenience to authors and readers.